Journal of Computer Sciences

Original Research Paper

Comparison of Classification Techniques on Fused Optical and SAR Images for Shoreline Extraction: A Case Study at Northeast Coast of Peninsular Malaysia

[1]Syaifulnizam Abd Manaf, [1]Norwati Mustapha,
[1]Md Nasir Sulaiman, [1]Nor Azura Husin and [2]Mohd Radzi Abdul Hamid

[1]*Faculty of Computer Science and Information Technology, Universiti Putra Malaysia, Serdang, Malaysia*
[2]*National Hydraulic Research Institute of Malaysia, Seri Kembangan, Malaysia*

Article history
Received: 02-04-2016
Revised: 26-10-2016
Accepted: 27-10-2016

Corresponding Author:
Syaifulnizam Abd Manaf
Faculty of Computer Science and Information Technology,
Universiti Putra Malaysia,
Serdang, Malaysia
Email: nizamkpt2020@gmail.com

Abstract: Shoreline is a very important element to identify exact boundary at the coastal areas of a country. However, in order to identify land-water boundary for a large region using traditional ground survey technique is very time consuming. Alternatively, shoreline can be extracted by using satellite images that minimizes the mapping errors. The trend of extracting shoreline has been shifted from image processing to machine learning and data mining techniques. By using machine learning technique, the satellite images could be classified into land and water classes in order to extract shoreline. However, the result is meaningless if it has cloud and shadow on the water-land boundary. In this study, we compare the accuracy and Kappa Coefficient of six machine learning techniques namely Maximum Likelihood, Minimum Distance, Mahalanobis Distance, Parallelepiped, Neural Network and Support Vector Machines on three type of images; single optical multispectral, single SAR and fused image. A case study for this research is done alongside Tumpat beach, located at the Northeast Coast of Peninsular Malaysia. All the machine learning techniques have been tested on the three types of images. The experimental results show that classification using SVM on single multispectral image has the highest accuracy among all. However, the classified of fused image using SVM is considered much more accurate because it can cater the cloud and shadow problem. Additionally, the classification on 5 and 10 m fused images also tested and the result shows that with the increase of spatial resolution of fused image, the classification accuracy also increases.

Keywords: Image Classification, Machine Learning, Image Fusion, Satellite Images, Shoreline Extraction

Introduction

Shoreline is the line where the land and water bodies meet and is called boundary separation between both (Boak and Turner, 2005; Dolan *et al*., 1991). In the coastal area, it is considered to be one of the most dynamic regions because it is mainly attributed to the natural Earth phenomena such as tide effect, wind speed, wind direction, sea level rise, natural disaster and anthropogenic processes (Mustaqim *et al*., 2014; Luu *et al*., 2015; Li, *et al*., 2002). Some parts of the shoreline are broken and need to be re-extract after the occurrence of natural disasters such as tsunamis and earthquakes (Al Fugura *et al*., 2011). Before shoreline is acquired, we have to determine the shoreline indicator which represents the true shoreline position. The shoreline indicators are categorized into three groups: Detectable visually features, tidal datum-based indicators and indicators based on processing method to extract shoreline (Boak and Turner, 2005; Li *et al*., 2002; Gens, 2010).

Acquisition of shoreline information is a fundamental work for addressing coastal accretion or erosion (Dolan *et al*., 1991). However, it is a time consuming, difficult and sometimes impossible task to extract shoreline from a large region when using traditional ground survey techniques, aerial photos and Global Positioning System (GPS) (Lipakis and Chrysoulakis, 2005). As pointed by many coastal scientists, investigating shoreline requires rapid and highly accurate methods that minimize the mapping errors (Rigos *et al*.,

2014). Alternatively, by using Earth observation techniques such as remote sensing for shoreline extraction is rapid and highly accurate thus minimizing the mapping errors. Moreover, remote sensing could provide a synoptic vision of the Earth whereby so large areas on the ground can be covered easily (Feng *et al*., 2014). Remote sensing could also offer a wide variety of image data with different spatial, spectral, radiometric and temporal resolution from optical multispectral or SAR images.

Many techniques are employed for extracting shoreline for middle to high resolution optical satellite images and SAR images from image processing techniques to image classification techniques using machine learning and data mining. For the satellite image processing techniques, methods used are band rationing (Sarwar and Woodroffe, 2013; Tarmizi *et al*., 2014; Lira and Taborda, 2014), edge detection (Al Fugura *et al*., 2011; Zhang *et al*., 2013; Wang and Allen, 2008), thresholding (Rigos *et al*., 2014), segmentation (Al Fugura *et al*., 2011; Shu *et al*., 2010; Zhao *et al*., 2012; Semenov *et al*., 2016), wavelet (Yu *et al*., 2013), cellular automata (Feng *et al*., 2014), raster color slicing (Tarmizi *et al*., 2014) and Normalized Difference Water Index (NDWI) (Choung and Jo, 2016). On the other hand, satellite image classification techniques (Lipakis and Chrysoulakis, 2005) were classified into supervised classification such as Maximum Likelihood (Muslim *et al*., 2006; Sekovski *et al*., 2014; Rokni *et al*., 2015), Parallelepiped (Sekovski *et al*., 2014), Minimum Distance (Sekovski *et al*., 2014), Mahalanobis Distance (Tarmizi *et al*., 2014; Sekovski *et al*., 2014), Neural Network (Rokni *et al*., 2015), Support Vector Machines (Rokni *et al*., 2015; Yousef and Iftekharuddin, 2014) and unsupervised classification such as ISODATA (Tarmizi *et al*., 2014; Sekovski *et al*., 2014). For the data mining method, association rules (Wang *et al*., 2010) and fuzzy (Dellepiane *et al*., 2004) were used.

The objective of the study is to compare classification techniques on single optical multispectral, single SAR and fused image for shoreline extraction. Section 2 reviews the existing methods for shoreline extraction from middle resolution to high resolution optical multispectral satellite images and SAR images. Section 3 discusses the study area and methodology of this research. Section 4 shows experimental results of fusion methods, classification methods and accuracy assessment for original multispectral, original Synthetic Aperture Radar (SAR) and fused image. Shoreline extraction from the fused image is also discussed. The conclusions and discussions are given in section 5.

Related Research

Single Image

In the past years, there were great amount of researches on middle resolution optical satellite images. Sarwar and Woodroffe (2013) used band ratio approach on Landsat TM and Landsat ETM images, using Band-5 divided by Band-2 to discriminate the water line on images. While Lira and Taborda (2014) also used band ratio of Band-4 (Red) divided by Band-5 (Near Infrared) to extract water/land boundary from Landsat 8 image. Frazier and Page (2000) implemented density slicing of the single mid-infrared band 5 of Landsat TM 5 and achieving an overall accuracy of 96.9%, a producer's accuracy for water bodies of 81.7% and a user's accuracy for water bodies of 64.5% using Maximum Likelihood. While, Yu *et al*. (2013) proposed a new algorithm on shoreline detection with non-separable wavelet and accurately extract the shoreline based on Distance Regularized Level Set Evolution (DRLSE). Zhang *et al*. (2013) demonstrated by using low-precision satellite images of multisource image matching algorithm with SIFT operator, the coastline could be extracted by the edge detection method. Feng *et al*. (2014) proposed a Cellular Automata (CA) algorithm to extract shorelines from multi-temporal Landsat TM images of Shanghai Municipality of China for year 1979 to 2008 by analysing the edge directional information of the images. Wang *et al*. (2010) discovered the association rules of the sea-land separation from learning samples by using the class association rule algorithm. Then, the sea and the land of the image were separated with the mined rules. Recently, Choung and Jo (2016) proposed shoreline change assessment using NDWI map of Landsat TM 5 images for various types of coasts such as sandy, rocky and hoary whereby shorelines were extracted from each NDWI map through the thresholding method for separating black and white regions of grey-level imagery. Rigos *et al*. (2014) performed an empirical image thresholding process. Then, they employed the Chebyshev polynomials to approximate the histograms of the resulting images. Finally, the third module applies an RBF network. Recently, Semenov *et al*. (2016) propose an algorithm using edge and contour-point information on NOAA Advanced Very High Resolution Radiometer (AVHRR) to discriminate shorelines.

The technology advancement of satellite sensors which provide high resolution images for the past two decades has attracted many researches to focus on it. Lipakis and Chrysoulakis (2005) used machine learning algorithms which exploits both the spectral and spatial information to extract shoreline. Moreover, they also found the accuracy extracted shoreline depend on the image orthorectification and image classification. Muslim *et al*. (2006) proposed two techniques such as geostatistical two-point histogram and super resolution pixel-swapping algorithm which could be used by Maximum Likelihood to accurately extract shoreline of IKONOS images. Sekovski *et al*. (2014) found the optimal bands for distinguishing land/water transition is the combined use of WorldView-2 spectral bands 1/2/7/8 or 1/2/4/7/8 allowed a successful delineation of the

wet/dry transition area. ISODATA achieved good results in detecting water bodies when compared to 4 other supervised classification methods; Parallelepiped, Gaussian Maximum Likelihood, Minimum-Distance-to-Means and Mahalanobis Distance and ISODATA unsupervised classification ISODATA approaches in delineating wet/dry part of proxy-based shoreline by processing high-resolution multispectral WorldView-2 satellite imagery. Tarmizi *et al*. (2014) demonstrated that Mahalanobis distance and ISODATA techniques most accurately from the other two techniques, Raster Color Slicing and Band Rationing on Quickbird images which employed Near Infrared (NIR) and visible band in detecting shoreline. It was found that only the shoreline bordering sandy beach and vegetation area can be selected as the correct shoreline as they were very close in term of approximate position of high water line that has been quantified through qualitative and quantitative measures.

Another attempt made beside multispectral optical satellite is the analysis of SAR images. Al Fugura *et al*. (2011) proposed a series of processes including filtering, enhancements and image segmentation to extract RADARSAT-1 satellite image. The purpose of filtering was to overcome inherent speckle noise due to the environmental conditions at the time of the image acquisition which happen when random noise over the sea surface. Enhancement process was the contrast between land and water and further applied with Sobel and Linear edge detections. Grey-level segmentation with pixels with similar grey values in a nearby region and clustered as the same object to achieve separation between land and water. The approach proposed by Dellepiane *et al*. (2004) was based on fuzzy connectivity concepts in combining uniformity features and the averaged image of ERS-1 and ERS-2 images. The extracted coastlines have proved that the coherence image is an important feature to separate land and sea. Hence, the results do not depend on spatial resolution that potentially could implement any type of satellite image resolution in the future. Shu *et al*. (2010) extracted shoreline along Canadian Pacific coast from RADARSAT-2 Fine mode with narrow band level set segmentation method. Zhao *et al*. (2012) proposed an improved CV Level Set method to segment different kind of SAR images such as Radarsat-1, Cosmo-Sky Med and TerraSAR-X in extracting shoreline. Wang and Allen (2008) created a model to implement Sobel edge detection beside focal filtering and differencing operations on JERS-1 L-HH SAR data in delineation of shorelines in 1994 and 2006.

Fused Images

For the fused image, Rokni *et al*. (2015) proposed a new technique to integrate pixel level image fusion and image classification techniques in detecting change on water surface of Lake Urmia in Iran. The proposed approach showed the effectiveness especially for Gram Schmidt-ANN and Gram Schmidt-SVM fusion classification. Yousef and Iftekharuddin (2014) proposed an approach using fused image of LIDAR Digital Elevation Model (DEM) data and aerial images to extract Mean High Water (MHW) shoreline without reference to a tidal datum which classified into land and water using SVM classifier.

Materials and Methods

The current methodology is constructed based on satellite image classification approach and it is considered as a complex process. Here is the methodology employed in the current research as shown in Fig. 1. The major steps of image classification of remotely sensed images may include identifying study area, choosing suitable satellite image, pre-processing, selection of training and testing samples, selection of suitable machine learning image classification methods, post-processing and accuracy assessment (Choung and Jo, 2016; Sekovski *et al*., 2014). However, this research requires extra steps in pre-processing stage that is identification of shoreline definition and additional phase, image fusion stage with perform image fusion methods before moving into image classification stage. After performing accuracy assessment, post-processing is the final stage to extract shoreline from classified image. For detailed analysis, post-processing sub-processes such as sieve and clump, classification to vector and polygon to polyline processes should be performed.

Study Area

The chosen study area is located in the district of Tumpat, Kelantan as shown in Fig. 2. Specifically, this area extends from the Southern Thailand border to the border of Tumpat-Kota Bharu district and it was approximately 33 km kilometers long. Its geographic location starts at latitude 456 030 to 473 220 E and the longitude starts from 689 730 to 682 830 N. At the beginning, the shoreline is relatively straight and it is curvy at the end. The coast is wholly sandy, built up by deltaic, marine and swamp deposits. There is no island located off the coast. Thus, exposing it directly to the waves from the South China Sea and the Gulf of Thailand (TiongSa and HuiBoon, 2010).

The coast of Tumpat is located at the East coast of Peninsular Malaysia which is the area most affected by flooding, coastal erosion, etc. from the northeast monsoon season that occurs in November till March. This monsoon brings rain to the west coast of Malaysia Peninsular. There is also the Kelantan river that flows to the South China Sea with a catchment area of about 11900 km^2. The rainfall over the area varies between 0 to 1750 mm (MatAmin *et al*., 2012). This area is chosen because of projected of Sea Level Rise (SLR) for the

year 2100 is 5.2 to 5.7 mm/year which is the highest at the East Coast of Peninsular Malaysia and among the highest in Peninsular Malaysia (Awang and Hamid, 2013). Moreover, for broader climate, during (boreal) winter of the East Asian-Western Pacific monsoon, the northeast wind causes a sea level surge in the Gulf of Thailand and along the east coast of Peninsular Malaysia (Luu *et al*., 2015; Hague, 2015).

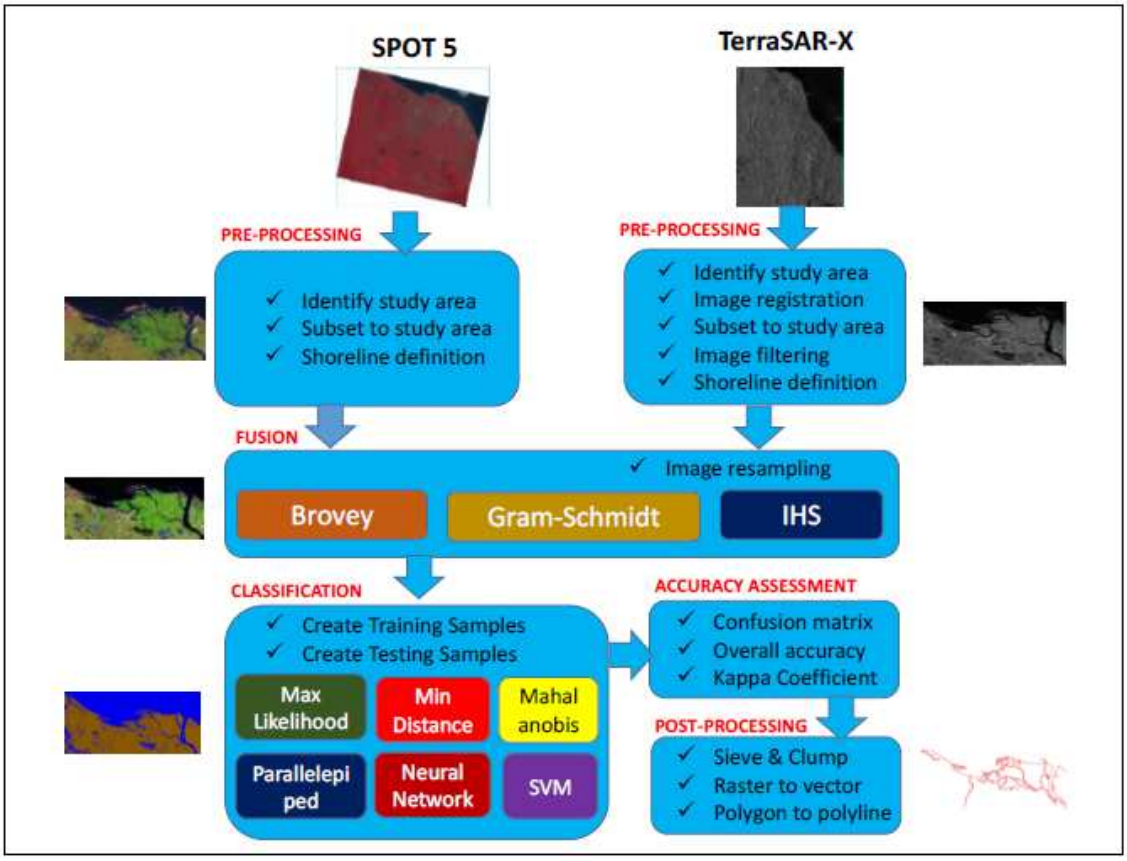

Fig. 1. Methodology on current research

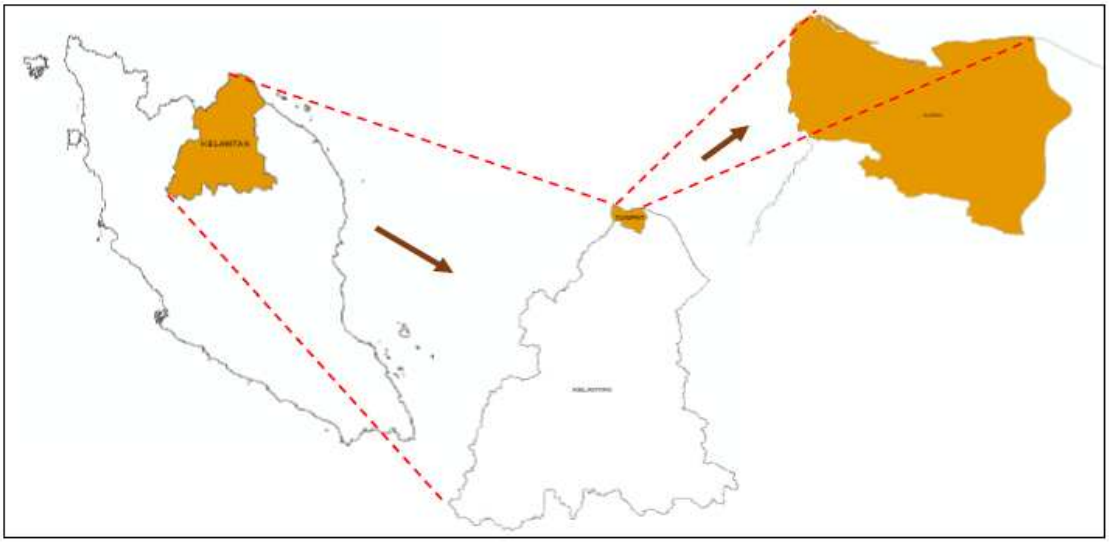

Fig. 2. Study area

Airborne Data Acquisition

Two images were chosen in this study, one scene of optical SPOT 5 Multispectral (MS) image and another scene of Terra SAR-X image were acquired from Malaysian Remote Sensing Agency. The SPOT 5 MS was acquired on 5 Feb 2014 while the SAR image was acquired on 10 Dec 2013. The original spatial resolutions for both SPOT 5 MS and SAR images were 10 and 18.5 m respectively. The detail of image acquisition is shown in Table 1.

The ancillary data used in this study included land use map from the Federal Department of Town and Country Planning and Digital Terrain Model (DTM) from the Department of Survey and Mapping Malaysia, which were used to assist the interpretation and analysis processes.

Pre-Processing

In applying optical and SAR fusion, SPOT 5 level 2 is set to be a base reference because it has coordinates. RSO Malaya Meter is chosen as the base coordinate's reference system. Then, SAR is geo-referenced by performing image to image registration with the SPOT 5 that already has coordinates. Each image will be subsetted to the study area that has already been defined such as district boundary as shown in Fig. 3 and 4.

Image Fusion

Image fusion is a technique that combines two or more images to produce a new image that preserves the desired information. The image to be combined has to be captured in the same region or study area. These images can be recorded by using different sensors, at different time periods or with different spatial and spectral features (Sarup and Singhai, 2011).

Before performing image fusion, each image has to be checked for its spatial resolution. Normally there is one image which will have a higher spatial resolution than the other image. In our case, the spatial resolution of SPOT 5 image is preserved to 10m resolution while SAR data were resampled to 5, 10 and original 18.5 m using Nearest Neighbor resampling algorithm. There are other methods that can be employed to resize an image whether to enlarge, reduce or preserve to the original size besides Nearest Neighbor such as Bilinear Interpolation and Cubic Convolution. The underlying mechanism behind resampling image is a process by which new pixel values are interpolated from existing pixel values during datum transformation, map projection or resizing operations (Gurjar and Padmanabhan, 2005). The effect of image resampling is a change in number of rows and columns which affect image quality such as how closely the interpolated value matches the original value of each pixel (Foody, 2002).

Fig. 3. Original SPOT 5 image after subset to study area

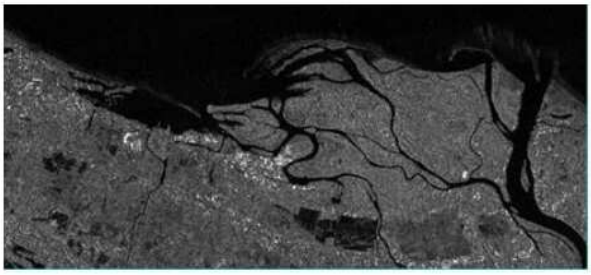

Fig. 4. Original TerraSAR-X image after subset to study area

Table 1. Data acquisition

	Image characteristics		
Images	Path/Row	Date	Resolution
SPOT 5	269/339	5 Feb 14	10 m
TerraSAR-X	ScanSAR 009 HH	10 Dec 13	18.5 m

Image fusion can be implemented by using numerous techniques. According to Gungor and Shan (2006), image fusion methods can be classified into three main groups according to their mathematical models. The standard image fusion techniques based on color theory consists of Brovey, Intensity, Hue and Saturation (IHS) and Multiplicative methods. However, Mandhare *et al*. (2013) classified it depending on the stage which fusion takes place; namely pixel level, feature level and decision level.

Brovey is also called the color normalization transform for the involvement of Red-Green-Blue (RGB) color transform method. It is a combination of arithmetic operations and normalizes the spectral bands before multiplied with higher resolution image such as panchromatic or SAR. It retains the corresponding spectral feature while all the luminance information is transformed into high resolution image (Mandhare *et al*., 2013). In order to implement it, each SPOT band is multiplied by a ratio of the SAR band divided by the amount of the SPOT bands.

The IHS methods used RGB color space commonly which is not fit for an integration process as the relationship of the image channels is not clearly highlighted. The IHS system offers the advantage that

the separate channels outline certain color properties, namely intensity, hue and saturation (Tu *et al*., 2004). In applying the IHS method, each of the three bands of SPOT image is categorized blue, green and red, respectively. These color components are then transformed into intensity, hue and saturation components using the color space mapping model. The next step is replacement of the intensity component by the SAR image. Finally, an inverse transformation from IHS to RGB is conducted to obtain the composite image, which has both rich spectral information and high spatial resolution.

In the case of Gram Schmidt algorithm, to merge two images, a Terra SAR-X band is simulated from the SPOT MS bands. It is obtained by averaging the bands of multispectral image. A Gram Schmidt transformation is then executed to the simulated SAR and multispectral bands. Next, the SAR band is replaced with the first Gram Schmidt band. Finally, an inverse Gram Schmidt transformation is applied to form the fused image.

Training and Testing Sets

In machine learning, training set is created to build the model while testing set is created to measure its performance. Training and testing sets of polygons are created which each set consisting of two classes, one that corresponds to water elements and another one that corresponds to land elements. Ground reference data could be used to pick both training and testing areas. Band combinations also play an important role to select both training and testing area visually. This is the most important step because the quality of the results is dependent on the quality of the training and testing sets. Moreover, spectral properties of training sample class are examined to identify signature profile of a class (Apan *et al*., 2002). After creating both sets, separability of the sets are calculated based on Jeffries-Matusita distance and Transformed Divergence (Bochow, 2005). If the result is close to 2.0 this will indicate perfect separability while values less than 1.6 indicate less separability with the classes are quite similar. In other word, separability is a measurement for which patterns can correctly associate with their classes statistically. The training and testing polygon can be shown as in Fig. 5 and 6 respectively.

Image Classification

The intent of the classification process is to map the land and water body classes as an indicator of shoreline extraction later. Each class has different spectral signatures as it absorbs and reflect different wavelengths (Sekovski *et al*., 2014).

After that, image classification technique is employed to the filtered fused image. There are six machine learning algorithms applied in classifying the satellite image such as Mahalanobis Distance (Chennai *et al*., 2015), Minimum Distance (Chennai *et al*., 2015), Maximum Likelihood (Ahmad and Quegan, 2012), Parallelepiped (Lü and Tang, 2012; Vanitha *et al*., 2013), Neural Network (Ojaghi *et al*., 2015; Mustapha *et al*., 2010) and Support Vector Machines (Petropoulos *et al*., 2011).

The minimum distance classifier is applied to classify unknown data to classes which minimize the space between the data and the class in multi-feature space. The distance is defined as an index of similarity so that the minimum space is identical to the maximum similarity.

Mahalanobis distance is similar to minimum distance, except that the covariance matrix is applied instead. Unlike minimum distance, this method considers the variability of classes into account. It relies heavily on a normal distribution of the data in each input set.

Maximum likelihood is based on the probability that a pixel belongs to a particular class. The basic theory assumes that these probabilities are equal for all classes and that the input bands have normal distributions. It is to estimate the likeliness of each pixel point by point and this pixel is assigned to the class corresponding to the maximum likelihood. It does not consider class variability.

Parallelepiped classifier divides each axis of multi-spectral feature space. The decision region for each class is defined on the basis of a lowest and highest value on each axis. The accuracy of classification depends on the selection of the lowest and highest values in consideration of the population statistics of each class.

Artificial Neural Network (ANN) is the most common approach of nonparametric classification. There are different types of ANNs. An ANN is characterized by its architecture, training or learning algorithm and its activation function. The architecture of the ANN models used consists of the following: An input layer, one hidden layer and an activation function.

The SVM is a form of statistical learning method based on small samples. It examines how to construct a learning machine, to make the pattern classification. The basic idea under the SVM method is to transform the input features into a higher-dimensional space where the two classes can be linearly separated by a high-dimensional surface, known as a hyper-plane.

Accuracy Assessment

In order to evaluate the percentage of correctly classified or matched pixels, the post classification accuracy assessment is carried out. The quality of shoreline depends on the classification accuracy and on the type of information represented on the map. The accuracy of the generated map can be described on the basis of the completeness of the map and the thematic precision of the information illustrated on the map. The confusion matrix was used to observe the effectiveness of the classification map. The confusion matrix is a cross-tabulation of the classified and actual class labels for the study area. It characterizes the correlation among two samples of measurements taken from the classified area.

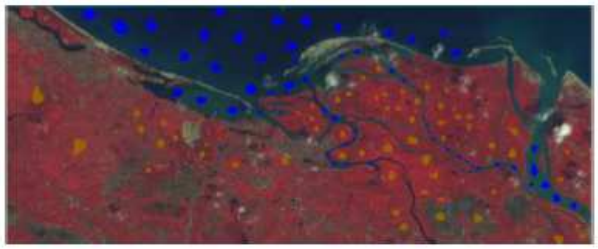

Fig. 5. Training set of polygons

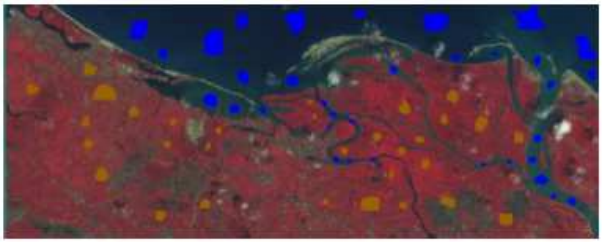

Fig. 6. Testing set of polygons

With the use of the confusion matrix, measurement such as overall accuracy, user accuracy, producer accuracy and Kappa Coefficient can be calculated (Foody, 2002; Gao and Xu, 2014; Huang *et al*., 2002). The overall accuracy is determined by dividing the cumulative of the main diagonal items of the confusion matrix by the entire number of samples.

Post-Processing

In the last step, the result of classified image will convert from raster to vector format. Before converting to vector the classified image has to perform sieve and clump processes to generalize that data. Then, raster to vector operation is applied which will result in polygons that is smooth and not curvy. After that, polygon feature to line conversion is applied so that will result in line vector format. The line is then edited and any erroneous data is deleted so that the cleaned vector lines haves to go through a smoothing process resulting in less spiky and smoother in appearance. As a result, the new line produced is selected and considered as the best approximation to the position of the shoreline.

Results and Discussion

Experimental Setup

The type of satellite image used in this work need to be identified before performing any further process. In this study, we used two type of images, namely MS optical and SAR images. In pre-processing stage, each image need to undergo pre-preprocessing process until both images were fitted with the same coordinate system in order to overlay each other. The pre-processing steps for both images were similar except SAR image. Two additional process need to be performed in SAR image such as image to image registration and image filtering. In fusion stage, both images were fused together in order to create a new higher resolution image. There are 3 fused algorithm applied, namely Brovey, Gram-Schmidt and IHS. For each fused image, we calculated the correlation coefficient in order to compare with the original image. The image has result near to 1.0 was chosen to the next stage for classification process. There are 3 spatial resolution considered for image fusion, 10, 18.5 and 5 m. In classification stage, we created 68 and 75 polygons of training samples on the fused image for land and water classes respectively. For testing samples, we created 30 and 35 polygons for land and water classes respectively. Image classification was performed on the fused image resulting a classified image of land and water classes. There are 6 classification algorithms used in this study such as Maximum Likelihood, Minimum Distance, Mahalobis Distance, Parallelepiped, Neural Network and Support Vector Machine. 6 types of image based on their spatial resolution such as 10, 18.5 and 5 m for single image and 10, 18.5 and 5 m also for fused image are considered. The performance of the experiments was assessed in terms of overall accuracy and Kappa Coefficient using testing samples created before. In post-processing stage, generalization processes such as sieve and clump were employed. Finally, 2 conversion processes namely raster to vector conversion and polygon to polyline conversion in order to obtain a final extracted shoreline.

Fusion Result

The results of the image fusion methods applied to merge the SPOT 5 multispectral and SAR images are shown in Fig. 7-9. Based on visual interpretation, the fusion results show that the shoreline is well detected in the Gram-Schmidt fused image. However, the Gram-Schmidt and Brovey also generated too much noise at the area of water bodies. The most suitable image fusion is IHS because it does not generate too much noise and it can produce almost similar to the original image.

For the quality assessment of fused images, we use Correlation Coefficient (CC) to measure similarity between two images and it is defined as:

$$CC(A|B)=\frac{\sum_{i=1}^{M}\sum_{j=1}^{M}\left(A_{i,j}-\overline{A}\right)\left(B_{i,j}-\overline{B}\right)}{\sqrt{\sum_{i=1}^{M}\sum_{j=1}^{M}\left(A_{i,j}-\overline{A}\right)^{2}\left(B_{i,j}-\overline{B}\right)^{2}}} \quad (1)$$

where, M × N is the image's size, A and B are the mean of images A and B. CC of band 432 of fused images is used in this study to quantitatively assess the fused images produced using the image fusion algorithms as calculated in Table 2.

Fig. 7. SPOT5 and SAR fusion using Brovey, RGB=432

Fig. 8. SPOT 5 and SAR fusion using Gram-Schmidt, RGB=432

Fig. 9. SPOT5 and SAR fusion using IHS, RGB=432

Table 2. Correlation coefficient of original and fused images

	Correlation coefficient		
Images	R	G	B
Original SPOT 5 MS	1	1	1
Original TerraSAR-X			
Brovey, RGB=432	0.86	0.48	0.73
Gram Schmidt, RGB=432	0.77	-0.13	0.15
IHS, RGB=432	0.87	0.51	0.73

Kappa Coefficient is a coefficient that demonstrates a computable measurement using statistical relationships between the original and fused images, the better the estimation of the spectral values (Nikolakopoulos, 2008). The ideal value of correlation coefficient is 1. From the result, the IHS fused image is more correlated to the original SPOT image.

Classification and Accuracy Assessment Outcome

This section will describe further analysis into the classification and accuracy assessment result. There are two classification scenarios namely classification on single image and fused image. Table 3 and 4 shows the classification accuracy and Kappa Coefficient for both scenarios.

Classification on Single Image

Classification on single image will be divided into two main groups which are original multispectral image and SAR image.

Classification on Original Multispectral Image

For original MS image, SPOT 5 was used and the spatial resolution of SPOT 5 MS was 10 m. The output after performing the stated six machine learning algorithms on single SPOT 5 MS image is shown in Fig. 10 is while original image of SPOT 5 is shown in Fig. 11.

Overall accuracy and Kappa Coefficient of SPOT 5 MS original image for all machine learning algorithms recorded the best for all three images, SPOT 5 original, SAR original and resampling SAR.

SVM achieved the best classification result of all machine learning algorithms with overall accuracy of 99.9723% while parallelepiped is the worst with 98.1269% to classify land and water bodies.

Even though the classification of original SPOT 5 image obtained the highest classification accuracy, however there are eight errors identified as shown in Fig. 10. Seven areas identified as A to G have classification errors due to cloud while another one area (H) due to shadow. From the first sight, the spotted A-G areas looked like “land” and H area looked like “water”.

Classification on SAR Image

For SAR image, TerraSAR-X ScanSAR was used. The original spatial resolution for Terra SAR-X is 18.5 m. From a practitioner point of view, the experts from Malaysia Remote Sensing Agency suggested that Terra SAR-X Scan SAR could be resampled to 5m spatial resolution. Therefore, it was also considered to be evaluated in this study.

In term of accuracy assessment for SAR image, it can be shown that the classification accuracy of resampling SAR (5 m) slightly better than original SAR. For resampling SAR, SVM was considered the best machine learning algorithm with overall accuracy 97.4792% and Kappa Coefficient 0.9478 while both Mahanalobis Distance and Minimum Distance recorded the worst machine learning algorithms with overall accuracy 94.5321 and Kappa Coefficient 0.8850 achieved. However, for original SAR image, Neural Network was the best with 97.0183% and Kappa Coefficient was 0.9453.

Unlike the original SPOT 5 image, SAR cannot interfere with cloud and shadow. Therefore, the classification results are promising.

Fig. 10. Image classified into land and water by single SPOT MS image

Fig. 11. Original SPOT 5 MS with 10% cloud and shadow

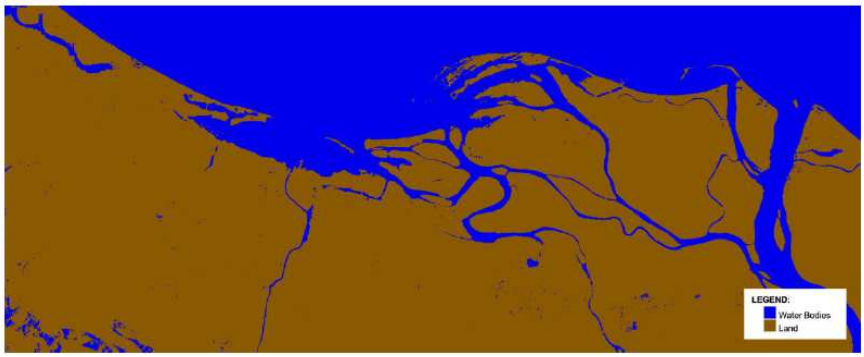

Fig. 12. Image classified into land and water by fused image

Fig. 13. Fused image using IHS method with no cloud and shadow

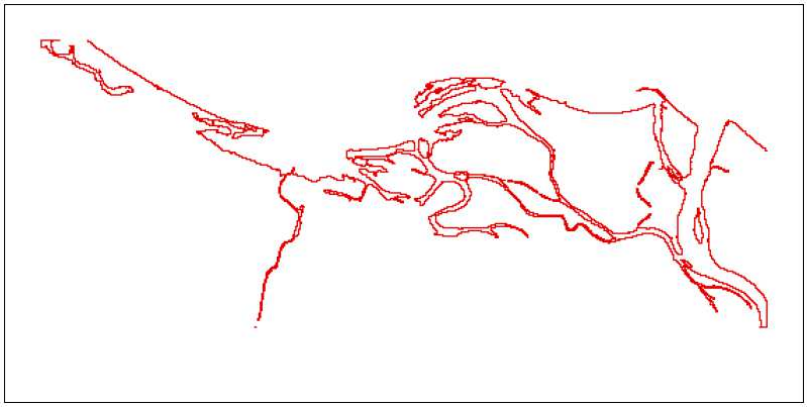

Fig. 14. Extracted shoreline output

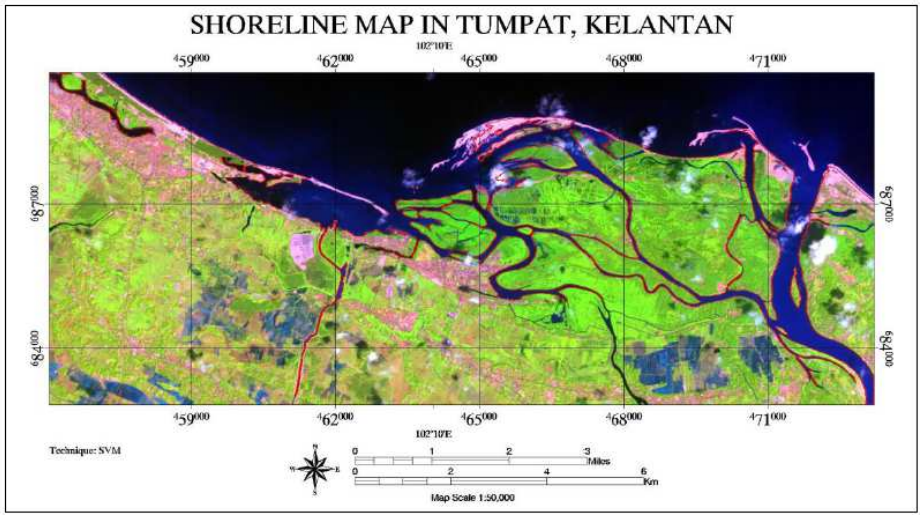

Fig. 15. Shoreline map

Table 3. Classification accuracy assessment on single and fused images

	Single image			Fused image		
Machine learning algorithm	Original SPOT 5 MS (10 m)	Original SAR (18.5 m)	Resampled SAR (5 m)	IHS SPOT + SAR (18.5 m)	IHS SPOT + SAR (10 m)	IHS SPOT + SAR (5 m)
Mahanalobis distance	98.6458	94.4409	94.5321	94.4852	94.5695	94.5911
Maximum likelihood	99.7614	96.2436	97.2409	98.8629	99.6326	99.5921
Minimum distance	98.6375	94.4409	94.5321	94.7884	94.7864	94.7933
Neural network	99.9057	97.0183	97.3681	99.6399	99.6932	99.5533
Parallelepiped	98.1269	95.7991	96.2286	96.2539	97.3776	97.4947
Support vector machine	99.9723	96.3866	97.4792	99.1409	99.5818	99.7071

Classification on Fused Image

For fused image, three fused images used namely SPOT 5 MS (10 m) fused with single original SAR image, SPOT 5 MS fused with single 10 m SAR image and SPOT 5 MS fused with single 5 m SAR image were considered for classification.

For the classification accuracy assessment on the fused image, most machine learning algorithms perform good if fused with 5 m SAR except for Maximum Likelihood and Neural Network which both perform good if fused with 10 m SAR. The best machine learning algorithm for classification of fused SPOT 5 MS and SAR was SVM which overall accuracy of 99.7071 and Kappa Coefficient 0.9940 if fused with 5 m resolution. While the worst machine learning algorithm for the same case was Mahalanobis Distance which fused with original SAR image.

Table 4. Kappa coefficient on single and fused images

	Single image			Fused image		
Machine learning algorithm	Original SPOT 5 MS (10 m)	Original SAR (18.5 m)	Resampled SAR (5 m)	IHS SPOT + SAR (18.5 m)	IHS SPOT + SAR (10 m)	IHS SPOT + SAR (5 m)
Mahanalobis distance	0.9729	0.8836	0.8850	0.8845	0.8861	0.8862
Maximum likelihood	0.9952	0.9235	0.9327	0.9766	0.9924	0.9916
Minimum distance	0.9727	0.8836	0.8850	0.8910	0.8907	0.8906
Neural network	0.9981	0.9382	0.9453	0.9926	0.9937	0.9908
Parallelepiped	0.9632	0.9128	0.9217	0.9232	0.9463	0.9487
Support vector machine	0.9994	0.9249	0.9478	0.9823	0.9914	0.9940

After classifying the fused image, the output shown in Fig. 12. From visual interpretation, the classified result can clearly show the difference between land and water classes. As compare with actual images as in Fig. 13 together with the classification accuracy assessment results, the fused image showed the best output.

Shoreline Output

The classified image was chosen from the best fused image in term of accuracy, Kappa Coefficient and visual interpretation for shoreline extraction later. Proper post-processing tasks were performed on the chosen classified image such as sieve and clump to avoid result with very curvy polygon. After performing raster to vector conversion on that image, a polygon was created to be used after that. Finally, polygon to polyline conversion was employed to result a shoreline as shown in Fig. 14 that can be used for further shoreline map analysis as shown in Fig. 15. The shoreline can be shown via red line overlaying the original SPOT 5 MS image.

Conclusion

We have presented the comparison of the image classification methods using six machine learning techniques such as Maximum Likelihood, Minimum Distance, Mahalanobis Distance, Parallelepiped, Neural Network and Support Vector Machines on original SPOT 5 MS image, original SAR image and fused image. However, for the fused image, 3 comparisons were done for fusion of SPOT 5 MS with three resolutions of SAR such as original SAR (18.5 m), fusion of SPOT 5 MS with 10 m SAR and fusion of SPOT 5 MS with 5 m SAR.

Among the three fusion approaches, namely Brovey, Gram-Schmidt and IHS, IHS approach was chosen because it was more correlated to the original SPOT 5 MS image evaluated using correlation coefficient calculation. Later, it was used to classify land and water body classes in order to extract shoreline.

In classifying land and water boundary, SPOT 5 MS image was the best in term of the accuracy and Kappa Coefficient for single image. However, the single SPOT 5 MS has cloud and shadow on the water and land boundary that resulted in error for extraction of shoreline later. Therefore, the best classification accuracy next to single SPOT 5 MS was fused SPOT 5 MS and SAR.

For the fused image, the classification result of fused image with higher spatial resolution was the best except for Maximum Likelihood and Neural Network which both worked best if fused with 10 m SAR. The best machine learning algorithm for classification of fused SPOT 5 MS and SAR was SVM which worked best if fused with 5 m resolution. While the worst machine learning algorithm for the same case was Mahalanobis Distance which fused with original SAR image.

From the study, we identified by using fused image, extra pre-processing task as cloud and shadow removal is not needed because it has disappeared after merging two images. The results of the study also can be utilized as a new method to map shoreline for coastal zone regions to quantify the extent and to aid future prediction studies which helps coastal agencies to develop sustainable coastal practices. The change in the position of the shoreline could be used to determine if the changes are mainly natural or anthropogenic effect.

For the future work, this research could be extended with high resolution multispectral images such as Quickbird, IKONOS, WORLDVIEW, etc. satellite images. Moreover, ensemble learning or deep learning methods have potentials to be applied for higher accuracy shoreline extraction.

Acknowledgement

This work is supported by Science Fund Research Grant funded by the Malaysian Government through Ministry of Science, Technology and Innovation (No: 01-01-04-SF2291). We also would like to thank the Malaysian Remote Sensing Agency, the Federal Department of Town and Country Planning Peninsular Malaysia, the Department of Survey and Mapping Malaysia for specially giving us data. Also not to forget to the Universiti Putra Malaysia for giving us logistic to complete this research.

Author's Contributions

All authors equally contributed to this work.

Ethics

This article is original and contains unpublished material. The corresponding author confirms that the other author has read and approved the manuscript and no ethical issues involved.

References

Ahmad, A. and S. Quegan, 2012. Analysis of maximum likelihood classification on multispectral data. Applied Math. Sci., 6: 6425-6436.

Al Fugura, A., L. Billa and B. Pradhan, 2011. Semi-automated procedures for shoreline extraction using single RADARSAT-1 SAR image. Estuarine, Coastal Shelf Sci., 95: 395-400. DOI: 10.1016/J.ECSS.2011.10.009

Apan, A., R. Kelly, T. Jensen, D. Butler and W. Strong *et al*., 2002. Spectral discrimination and separability analysis of agricultural crops and soil attributes using aster imagery. Proceedings of the 11th Australasian Remote Sensing and Photogrammetry Conference, Sept. 2-6, Brisbane, Queensland, pp: 396-411.

Awang, N.A. and M.R.B.A. Hamid, 2013. Sea level rise in Malaysia. Int. Associat. Hydro-Environ. Eng. Res., 2: 47-49.

Boak, E.H. and I.L. Turner, 2005. Shoreline definition and detection: A review. J. Coastal Res. DOI: 10.2112/03-0071.1

Bochow, M., 2005. Improving class separability - a comparative study of transformation methods for the hyperspectral feature space. Proceedings of 4th EARSeL Workshop on Imaging Spectroscopy, (WIS' 05), pp: 439-447.

Chennai, I., M. Madhura and S. Venkatachalam, 2015. Comparison of supervised classification methods on remote sensed satellite data: An application in Chennai, South India. Int. J. Sci. Res., 4: 1407-1411.

Choung, Y.J. and M.H. Jo, 2016. Shoreline change assessment for various types of coasts using multi-temporal Landsat imagery of the east coast of South Korea. Remote Sens. Lett., 7: 91-100. DOI: 10.1080/2150704X.2015.1109157

Dellepiane, S., R. De Laurentiis and F. Giordano, 2004. Coastline extraction from SAR images and a method for the evaluation of the coastline precision. Patt. Recognit. Lett., 25: 1461-1470. DOI: 10.1016/j.patrec.2004.05.022

Dolan, R., S. Fenster, J. Michael and S. Holme, 1991. Temporal Analysis of shoreline Recession and Accretion. J. Coastal Res., 7: 723-744.

Feng, Y., Y. Liu and D. Liu, 2014. Shoreline mapping with cellular automata and the shoreline progradation analysis in Shanghai, China from 1979 to 2008. Arabian J. Geosci., 8: 4337-4351. DOI: 10.1007/s12517-014-1515-7

Foody, G.M., 2002. Status of land cover classification accuracy assessment. Remote Sens. Environ., 80: 185-201. DOI: 10.1016/S0034-4257(01)00295-4

Frazier, P.S. and K.J. Page, 2000. Water body detection and delineation with landsat TM data. Photogrammet. Eng. Remote Sens., 66: 1461-1467.

Gao, J. and L. Xu, 2014. An efficient method to solve the classification problem for remote sensing image. AEU-Int. J. Electron. Commun., 69: 198-205. DOI: 10.1016/j.aeue.2014.09.001

Gens, R., 2010. Remote sensing of coastlines: Detection, extraction and monitoring. Int. J. Remote Sens., 31: 1819-1836. DOI: 10.1080/01431160902926673

Gungor, O. and J. Shan, 2006. An optimal fusion approach for optical and SAR images. Symp. Q. J. Modern Foreign Literatures.

Gurjar, S.B. and N. Padmanabhan, 2005. Study of various resampling techniques for high-resolution remote sensing imagery. J. Ind. Society Remote Sens., 33: 113-120. DOI: 10.1007/BF02989999

Hague, T., 2015. Understanding tidal and non-tidal representation of numerical model using data relationship analysis in singapore regional waters. Proceedings of the 36 th IAHR World Congres, 28 Jun.-3 Jul., The Hague, pp: 1-7.

Huang, C., L.S. Davis and J.R.G. Townshend, 2002. An assessment of support vector machines for land cover classification. Int. J. Remote Sens., 23: 725-749. DOI: 10.1080/01431160110040323

Li, R., R. Ma and K. Di, 2002. Digital tide-coordinated shoreline. Marine Geodesy, 0419: 27-36. DOI: 10.1080/014904102753516714

Lipakis, M. and N. Chrysoulakis, 2005. Shoreline Extraction using Satellite Imagery. In: Beach Erosion Monitoring, Pranzini, E. and E. Wetzel (Eds.), Florence, Italy, pp: 81-96.

Lira, C. and R. Taborda, 2014. Advances in applied remote sensing to coastal environments using free satellite imagery. Adv. Coastal Marine Resources, 9: 77-102. DOI: 10.1007/978-3-319-06326-3

Lü, Q. and M. Tang, 2012. Detection of hidden bruise on kiwi fruit using hyperspectral imaging and parallelepiped classification. Proc. Environ. Sci., 12: 1172-1179. DOI: 10.1016/j.proenv.2012.01.404

Luu, Q.H., P. Tkalich and T.W. Tay, 2015. Sea level trend and variability around Peninsular Malaysia. Ocean Sci., 11: 617-628. DOI: 10.5194/os-11-617-2015

Mandhare, R.A., P. Upadhyay and S. Gupta, 2013. Pixel-Level image fusion using brovey transforme and wavelet transform. Int. J. Adv. Res. Electr. Electron. Instrumentat. Eng., 2: 2690-2695.

MatAmin, A.R., F. Ahmad, M. Mamat, M. Rivaie and K. Abdullah, 2012. Sediment variation along the east coast of peninsular Malaysia. Ecol. Quest., 16: 99-107. DOI: 10.2478/v10090-012-0010-6

Muslim, A.M., G.M. Foody and P.M. Atkinson, 2006. Localized soft classification for super-resolution mapping of the shoreline. Int. J. Remote Sens., 27: 2271-2285. DOI: 10.1080/01431160500396741

Mustapha, M.R., H.S. Lim and M.Z. Mat Jafri, 2010. Comparison of neural network and maximum likelihood approaches in image classification. J. Applied Sci., 10: 2847-2854. DOI: 10.3923/jas.2010.2847.2854

Mustaqim, M., B. Mohd and Z.Z. Ghazali, 2014. Wind influence towards shoreline movement at pantai sabak, Kelantan Darulnaim.

Nikolakopoulos, K.G., 2008. Comparison of nine fusion techniques for very high resolution data. Photogrammet. Eng. Remote Sens., 74: 647-659. DOI: 10.14358/PERS.74.5.647

Ojaghi, S., H. Ebadi and F.F. Ahmadi, 2015. Using artificial neural network for classification of high resolution remotely sensed images and assessment of its performance compared with statistical methods. Am. J. Eng. Technol. Society, 2: 1-8.

Petropoulos, G.P., C. Kontoes and I. Keramitsoglou, 2011. Burnt area delineation from a uni-temporal perspective based on landsat TM imagery classification using support vector machines. Int. J. Applied Earth Observat. Geoinformat., 13: 70-80. DOI: 10.1016/j.jag.2010.06.008

Rigos, A., O.P. Andreadis, M. M.I. Andreas and G.E. Tsekouras *et al*., 2014. Shoreline extraction from coastal images using chebyshev polynomials and RBF neural networks. Proceedings of the 10th IFIP WG 12.5 International Conference on Artificial Intelligence Applications and Innovations, Sept. 19-21, Rhodes, Greece, pp: 593-603. DOI: 10.1007/978-3-662-44654-6_59

Rokni, K., A. Ahmad, K. Solaimani and S. Hazini, 2015. A new approach for surface water change detection: Integration of pixel level image fusion and image classification techniques. Int. J. Applied Earth Observat. Geoinformat., 34: 226-234. DOI: 10.1016/j.jag.2014.08.014

Sarup, J. and A. Singhai, 2011. Image fusion techniques for accurate classification of remote sensing data. Int. J. Geomat. Geosci., 2: 602-612.

Sarwar, M.G.M. and C.D. Woodroffe, 2013. Rates of shoreline change along the coast of Bangladesh. J. Coastal Conservat., 17: 515-526. DOI: 10.1007/s11852-013-0251-6

Sekovski, I., F. Stecchi, F. Mancini and L. Del Rio, 2014. Image classification methods applied to shoreline extraction on very high-resolution multispectral imagery. Int. J. Remote Sens., 35: 3556-3578. DOI: 10.1080/01431161.2014.907939

Semenov, S.M., N.A. Abushenko and A.S. Chichigin, 2016. Discrimination of shorelines on satellite images from boundary-point and halftone information. Mapp. Sci. Remote Sens., 36: 245-255. DOI: 10.1080/07493878.1999.10642126

Shu, Y., J. Li and G. Gomes, 2010. Shoreline extraction from RADARSAT-2 intensity imagery using a narrow band level set segmentation approach. Marine Geodesy, 33: 187-203. DOI: 10.1080/01490419.2010.496681

Tarmizi, N., A.M. Samad, M. Safarudin, C. Mat and M. Shukri *et al*., 2014. Qualitative and quantitative assessment on shoreline data extraction from quickbird satellite images. IPASJ Int. J. Comput. Sci., 2: 54-62.

TiongSa, T. and Y. HuiBoon, 2010. 19.2 Malaysia - introduction. In: Encyclopedia of the World's Coastal Landforms, Bird, E.C.F. (Ed.), Springer Science and Business Media, Dordrecht, ISBN-10: 1402086385, pp: 1117-1128.

Tu, T.M., P.S. Huang, C.L. Hung and C.P. Chang, 2004. A fast intensity-hue-saturation fusion technique with spectral adjustment for IKONOS imagery. IEEE Geosci. Remote Sens. Lett., 1: 309-312. DOI: 10.1109/LGRS.2004.834804

Vanitha, A., P. Subashini and M. Krishnaveni, 2013. SAR Ice image classification using parallelepiped classifier based on gram-schmidt spectral technique. Comput. Sci. Inform. Technol., 9: 385-392. DOI: 10.5121/csit.2013.354

Wang, C., J. Zhang and Y. Ma, 2010. Coastline interpretation from multispectral remote sensing images using an association rule algorithm. Int. J. Remote Sens., 31: 6409-6423. DOI: 10.1080/01431160903413739

Wang, Y. and T.R. Allen, 2008. Estuarine shoreline change detection using Japanese ALOS PALSAR HH and JERS-1 L-HH SAR data in the Albemarle-Pamlico Sounds, North Carolina, USA. Int. J. Remote Sens., 29: 4429-4442. DOI: 10.1080/01431160801932525

Yousef, A. and K. Iftekharuddin, 2014. Shoreline extraction from the fusion of LiDAR DEM data and aerial images using mutual information and genetic algrithms. Proceedings of the International Joint Conference on Neural Networks, Jul. 6-11, IEEE Xplore Press, pp: 1007-1014. DOI: 10.1109/IJCNN.2014.6889863

Yu, S., Y. Mou, D. Xu, X. You and L. Zhou *et al*., 2013. A new algorithm for shoreline extraction from satellite imagery with non-separable wavelet and level set method. Int. J. Mach. Learn. Comput., 3: 158-163. DOI: 10.7763/IJMLC.2013.V3.293

Zhang, Y., X. Li, J. Zhang and D. Song, 2013. A study on coastline extraction and its trend based on remote sensing image data mining. Abstract Applied Analysis. DOI: 10.1155/2013/693194

Zhao, L., L. Fan, C. Wang, Y. Tang and B. Zhang, 2012. A non-supervised method for shoreline extraction using high resolution SAR image. Proceedings of the International Conference on Computer Vision in Remote Sensing, Dec. 16-18, IEEE Xplore Press, pp: 317-322. DOI: 10.1109/CVRS.2012.6421282